

Watching the Low-Frequency Motions in Aqueous Salt Solutions: The Terahertz Vibrational Signatures of Hydrated Ions

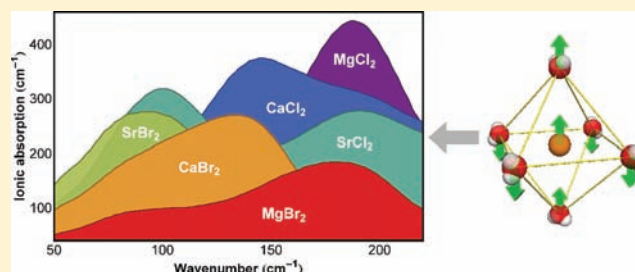
Stefan Funkner,[†] Gudrun Niehues,[†] Diedrich A. Schmidt,[†] Matthias Heyden,[‡] Gerhard Schwaab,[†] Karen M. Callahan,[‡] Douglas J. Tobias,[‡] and Martina Havenith^{*,†}

[†]Department of Physical Chemistry II, Ruhr-University Bochum, 44780 Bochum, Germany

[‡]Department of Chemistry, University of California, Irvine, Irvine, California 92697-2025, United States

S Supporting Information

ABSTRACT: The details of ion hydration still raise fundamental questions relevant to a large variety of problems in chemistry and biology. The concept of water “structure breaking” and “structure making” by ions in aqueous solutions has been invoked to explain the Hofmeister series introduced over 100 years ago, which still provides the basis for the interpretation of experimental observations, in particular the stabilization/destabilization of biomolecules. Recent studies, using state-of-the-art experiments and molecular dynamics simulations, either challenge or support some key points of the structure maker/breaker concept, specifically regarding long-ranged ordering/disordering effects. Here, we report a systematic terahertz absorption spectroscopy and molecular dynamics simulation study of a series of aqueous solutions of divalent salts, which adds a new piece to the puzzle. The picture that emerges from the concentration dependence and assignment of the observed absorption features is one of a limited range of ion effects that is confined to the first solvation shell.



INTRODUCTION

The nature of ion hydration is a fundamental question with many implications for specific ion effects that occur in a wide variety of phenomena in chemistry and biology, for example the specificity of protein channels that conduct ions across cellular membranes¹ or in describing ion transport in electrolytes,² which is a prerequisite for understanding electrochemical reactions. The systematic study of specific ion effects began over a century ago with Hofmeister's observations that the ability of salts to precipitate (salt out) or dissolve/denature (salt in) egg white and serum proteins depends on the nature of the constituent ions.^{3,4} Analogous specific ion effects occur in a wide variety of phenomena ranging from atmospheric science^{5,6} to biochemistry.⁷ Despite extensive research over many decades, an understanding of specific ion effects on the molecular scale remains a significant challenge.⁸ A crucial and still controversial issue that remains to be resolved is the extent to which ions influence the structure and dynamics of their surrounding water molecules. Previously, it was widely held that the Hofmeister series reflects the long-range structuring of water by specific ions (“structure makers” versus “structure breakers”), however ultrafast vibrational,⁹ X-ray absorption,¹⁰ new Raman,¹¹ and terahertz (THz) absorption¹² spectroscopy measurements suggest a lack of influence on the hydration dynamics beyond the first hydration shell. In contrast, current results from infrared photodissociation spectroscopy of gas-phase hydrated sulfate ions showed evidence for sulfate ion patterning (i.e., structuring) water beyond the first solvation shell.¹³ Decomposition of polarized Raman spectra in the OH

stretching region revealed an increase in the hydration shell with increasing anion size ranging from 4 to 11 H₂O molecules for F⁻ to I⁻, respectively.¹⁷ The assignment of the low-frequency spectrum of solvated anions to specific hydrogen bond vibrational modes formed between a halide ion (chloride, bromide, or iodide) and the surrounding water molecules (reported in ref 12) was also supported by ultrafast Kerr effect measurements of Heisler and Meech.¹⁴ A structuring, including a locking of the water network by cooperativity effects of particular combinations of ions, was proposed in a recent combined femtosecond (fs) IR and THz study.¹⁵ The argumentation was based on a model in which the fs IR studies are sensitive to the hydration dynamics of ions while the observed spectral features up to 1.5 THz were attributed to solvation water (affected by cations). However, using THz absorption spectroscopy we have now found evidence for specific anion **and** cation bands at frequencies between 50 to 250 cm⁻¹, which can be clearly assigned to vibrational modes of the ions along with their hydration shells. Our results reveal a strong coupling or strong interaction of both the anion and the cation with its first hydration shell, but do not support any long-ranged structure making, structure breaking, or cooperative effects for mono- and divalent salts.

We report a systematic study of the effects of hydrated ions on the network-coupled dynamics of water in divalent salt solutions using our unique high power p-Ge THz laser¹⁶ in

Received: August 22, 2011

Published: November 28, 2011

conjunction with precise wideband THz Fourier transform (FT) spectroscopy and MD simulations. We restricted our study to atomic anions and cations to avoid ambiguities due to coupling between intramolecular ion modes and the water network. The THz absorption depends linearly on concentration of each ion species, and their individual contributions are insensitive to the respective counterion. Whereas previous time-domain polarization-resolved coherent Raman scattering and time-domain THz measurements were assigned to either the hydrogen-bond stretching mode of the anion with the surrounding water molecules¹⁴ or the water rotational motion around the cation,^{15,17} respectively, we will demonstrate that for an interpretation of the THz spectrum both the hydrated cation and anion have to be taken into account.

NARROWBAND TERAHERTZ ABSORPTION

We can accurately determine changes in the absorption coefficient, α , of aqueous solutions with concentrations ranging from μM to M ^{18–20} using our precise narrow-band (2.3–2.8 THz, i.e. 76–93 cm^{-1}) THz absorption spectrometer. THz pulsed-laser radiation intensities were measured at several concentrations with neat water as a reference in a humidity and temperature controlled environment. Both reference and sample solutions were held in liquid cells with z-cut quartz windows and 50 μm Kapton spacers. To precisely separate solute-induced changes in the THz absorption from other contributions, we use the experimental setup from Figure S1 in Supporting Information (SI) to directly measure the difference of the averaged THz absorption coefficient of an aqueous salt solution and neat water between 2.3 and 2.8 THz rather than absolute numbers.

We observe that all aqueous solutions within the investigated concentration and frequency range show a linear absorption increase (with concentration). Hence, we treat the averaged THz absorption (between 2.3 and 2.8 THz) of these aqueous solutions as a linear combination of the absorption due to the sample and that of neat water. Here, we define the THz contribution due to the solvated ions as $\alpha_{\text{ion}} = \alpha_{\text{sample}} - \beta\alpha_{\text{water}}$ where α_{sample} and α_{water} are the calculated absorption coefficients using Beer's law and β is the ratio of the number of water molecules at a given concentration in an aqueous solution to that of neat water. The resulting THz ionic absorption coefficient α_{ion} for several alkaline earth halide salts is shown in Figure 1.

Within our experimental errors, we find no deviation from linearity up to high (3–4 M) concentrations. Thus, the observed THz absorption changes provide no indication of effects due to denser cation/anion packing as would be expected in the presence of any concentration-dependent cooperative effect between anions and cations. Rather, the lack of nonlinear contributions is consistent with independent oscillators formed by the ions and their solvation cage. In the case of longer-range ordering effects on the hydration dynamics we have found an onset of nonlinearity well below 3 M.¹⁸ We therefore, interpret the low-frequency spectrum of solvated salts in terms of collective ion–water vibrations which are restricted to the first solvation shell. This compares well with our work on monovalent salts¹² as well as with previous fs-IR spectroscopy studies.⁹

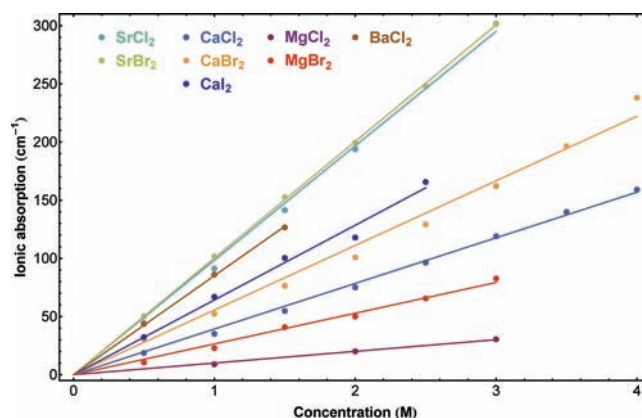


Figure 1. Ionic THz absorption (averaged between 2.1 and 2.8 THz) of divalent salts dissolved in water. The solid lines correspond to linear fits.

BROADBAND TERAHERTZ SPECTROSCOPY

To obtain the spectral response of the ions, we measured broadband THz FT spectra using a liquid cell with 40 μm Kapton spacers and diamond windows under nitrogen-purged and temperature-controlled conditions (20 ± 0.1 °C) in combination with a liquid-He cooled silicon bolometer. Since the first-order linearity also holds across the frequency range of our FTIR data (see SI), we can isolate the contribution of the ions in a similar fashion as with the narrow-band data. In Figure 2A we show as an example the frequency-dependent absolute absorption of 3 M aqueous MgCl_2 , neat water, and with β -scaled neat water. The inset of Figure 2A displays the resulting THz ionic absorption after subtraction of the scaled neat water spectrum from that of aqueous MgCl_2 . A compilation of the ionic contributions of 3 M solutions is shown in Figure 2B (the corresponding plot for monovalent ions can be found in the SI). We find an increase in the THz absorption for divalent salts compared to the monovalent moieties. Next, we shall demonstrate that the ionic spectrum (shown in Figure 2B for 3 M) can be dissected into **two** components that are attributed to the corresponding anion and cation motions along with their solvation shells.

When comparing the anion and the cation peaks for different divalent salts, one should keep in mind, e.g., that Mg^{2+} overlaps with the Cl^- band as well as the Sr^{2+} and the Br^- bands. In general we find an increase in intensity toward 200 cm^{-1} , i.e. toward the highest absorption of bulk water. This might be attributed to a residual water contribution in the spectra or might indicate a more efficient coupling of the ion bands with the bulk water network motions, leading to an increase in the ion bands.

We fitted the spectra of all salts at different concentrations to the sum of an anion and a cation absorption band using a damped, harmonic oscillator model.^{12,21} MgCl_2 is an exception, where the ionic absorption is best described by a single oscillator because the positions of the bands overlap. The resulting peak positions of the anion versus cation absorption bands of the divalent species are shown in Figure 3, which clearly supports our prior assumption of separable anion and cation peaks. As a general trend for both anions and cations, we find that the peak positions shift to lower frequency with increasing ion mass and decreasing charge density. According to the damped harmonic oscillator model¹² increasing ion masses would result in a decrease in the amplitude of oscillation

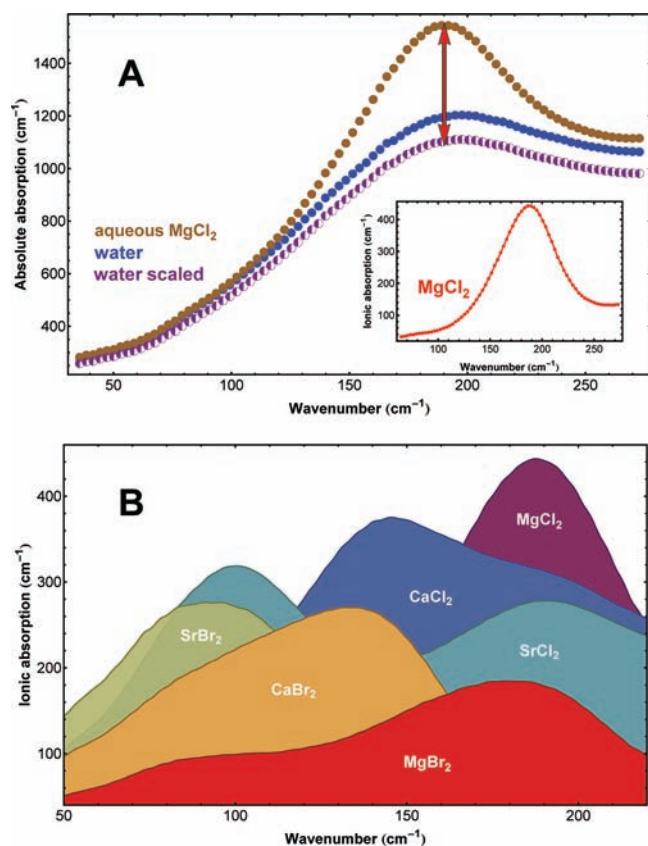


Figure 2. Terahertz ionic absorption bands. (A) the measured THz absorption of solvated MgCl_2 for a concentration of 3 M in the frequency range from 50 to 250 cm^{-1} (solid brown markers). When subtracting a scaled THz spectrum of neat water (open markers) from aqueous solutions we obtain the THz spectra of the ionic contributions (inset red markers) for divalent salts as plotted in (B). Each spectrum consists of two absorption peaks which are attributed to either the anion or the cation. For MgCl_2 both overlap.

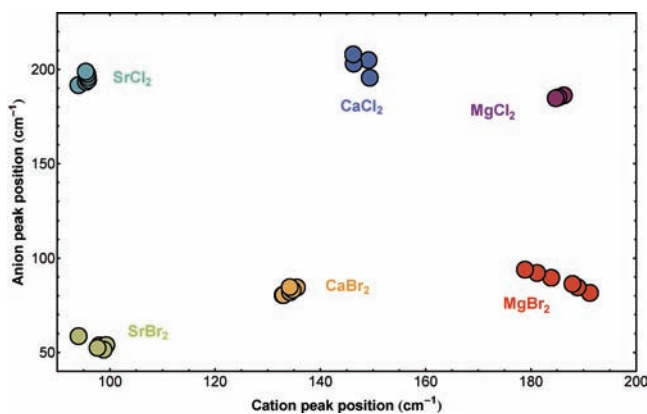


Figure 3. THz ionic absorption bands as shown in Figure 2B are fitted to two distinct absorption bands, one corresponding to the anion and one to the cation. Dots of the same color represent measurements on different concentrations ranging from 0.5 to 4 M.

and hence a decreased change of the induced dipole moment. This could be a further explanation for the general trend of increasing absorption peaks at higher frequencies (corresponding to smaller ion masses). Although the counterion masses and concentrations vary over a wide range, the center frequencies of the individual ion peaks remain remarkably constant. This

corroborates our narrow band frequency result of a strictly linear increase of ionic THz absorption with concentration. It supports the previous findings that the investigated ions show no long-range ordering effect on the water network.

MOLECULAR DYNAMICS SIMULATIONS

At this point, the identification of individual, well-defined anion and cation peaks justifies an attempt to assign the experimentally observed resonances to vibrational motions of the ions and water molecules in their solvation shells. For this purpose we carried out molecular dynamics simulations of the chloride and bromide solutions in water at 1 M of various divalent and monovalent cations (see SI for detailed simulation protocol). The polarizable POL3 force field for water has been employed in combination with established or in-house developed polarizable force fields²² for the ions. Among these simulations the Mg^{2+} solutions represent a special case. The number of water molecules in the solvation shell of each Mg^{2+} ion remained equal to six for each Mg^{2+} ion during the time scale of our simulations. In a previous study it was found that the residence lifetime of these water molecules in the first solvation shell of an Mg^{2+} ion can be estimated to be on the order of 9 μs and that contact ion pairs do not form in the concentration range studied here. As a consequence we can treat Mg^{2+} ions and their first solvation shell easily as molecule-like objects for the vibrational analysis of our simulations. This is further supported by the pronounced octahedral symmetry of the first solvation shell of Mg^{2+} ions, which was observed in our simulations.

For an octahedral system, symmetry dictates the presence of specific symmetry-adapted normal modes,²³ which describe all vibrations of the object. Such an analysis is a typical starting point for a vibrational analysis of a gas-phase molecules. However, the pronounced prevalence of the octahedral symmetry of the Mg^{2+} solvation shells convinced us to extend this kind of analysis to the condensed liquid phase in this case. While the exact mathematical definition of the symmetry-adapted normal modes of an octahedron is described in the SI, they describe, in general, six types of vibrational motions. According to their symmetric character, two of these can be assumed to be IR active, while three other vibrational modes are Raman active with varying intensities. The remaining vibrational mode is neither Raman nor IR active.

The IR active vibrational modes correspond to a motion of the central ion against a part of the octahedral solvation shell (see modes Θ and Ψ in Figure 4). In case of the Θ mode, the ion moves collectively with two water molecules on two opposing sides of the octahedron against the four remaining water molecules, which form a plane with the ion in its center. Instead, in the case of the Ψ mode, the ion moves collectively with these four water molecules against the latter two. The ion motion against part of its solvation shell involves a change of the dipole moment, which renders these modes IR active. Both IR modes are 3-fold degenerate.

The Raman active modes correspond to stretching motions of the ionic $\text{Mg}-\text{O}$ bonds, a fully symmetric and non-degenerate Φ mode and a 2-fold degenerate Ω mode (see Figure 4). The ρ and σ modes are both 3-fold degenerate, but only the latter involves a small change of the polarizability.

We used these symmetry-adapted normal mode coordinates to analyze the generated MD trajectories of the Mg^{2+} ions and their solvation shells within the simulated systems. Their motion has been projected onto these vibrational coordinates

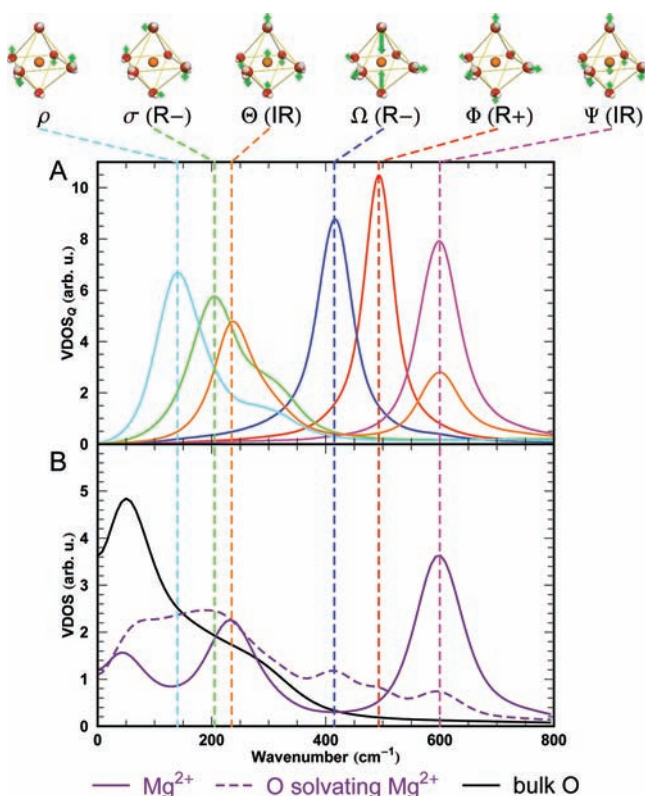


Figure 4. Symmetry-adapted octahedral normal modes for the Mg²⁺ ions and their octahedral solvation shells. IR, weak and strong Raman activities are denoted respectively as IR, R-, and R+. (A) Vibrational densities of states (VDOS) computed for the projected motion of Mg²⁺ ions and their first solvation shell along the symmetry-adapted normal modes. (B) VDOS computed from Fourier transformed velocity autocorrelation functions in Cartesian space for Mg²⁺ ions and the oxygens of solvating water molecules. For comparison also the VDOS of bulk water oxygens are shown.

Q_i to compute a spectrum in terms of the velocity time correlation formalism

$$\text{VDOS}_{Q_i}(\omega) = \frac{1}{2\pi} \int e^{i\omega t} \left\langle \dot{Q}_i(0) \dot{Q}_i(t) \right\rangle dt \quad (1)$$

which gives a vibrational density of states (VDOS) for the respective mode. The spectra computed from these projections are shown in Figure 4A. Apart from an imperfect separation of the two IR active modes, resulting in a second peak for the Θ mode at the frequency of the Ψ mode, each of the modes produces a clear spectrum with a specific resonance frequency.

We also find each of these modes in the vibrational density of states computed from Cartesian velocities of the Mg²⁺ ion and the oxygens of solvating water molecules as shown in Figure 4B. In correspondence with the properties of the assigned modes with respect to motion of the ion against its solvation shell, the VDOS computed from the Cartesian velocities of the ions themselves produces two pronounced peaks, which correspond to the IR active modes described above. Since each mode involves motion of water molecules relative to each other, we find for each of the assigned modes a corresponding resonance in the VDOS computed from the Cartesian velocities of the water oxygens in the first solvation shell (the inactive ρ and σ modes and the IR active Θ mode are not well separated, but the width of the corresponding peak in the VDOS suggests

the presence of several overlapping peaks in the corresponding frequency range).

The VDOS computed from the Cartesian velocities of the ion and the solvating water oxygens share an additional peak at roughly 60 cm⁻¹, which corresponds to the most dominant feature in the VDOS of water oxygens in bulk water. Recently, we have investigated the vibrational feature in pure water in an extensive ab initio MD study and found a pronounced collective character of the hydrogen bond bending, which is typically assigned to this frequency in bulk water. Our analysis showed that the underlying vibrations represent concerted motions of water molecules separated by as much as 5–6 Å or three hydrogen bonds.²⁴ The presence of this resonance in the VDOS computed from the Cartesian velocities of the Mg²⁺ ion and its solvating water molecules indicates that these collective vibrations are also present in the aqueous salt solution and involve motion of the solvated ions and their solvation shells.

For a comparison to the present experiment, the IR active Θ mode is of particular interest in the set of identified symmetry-adapted normal mode vibrations of the Mg²⁺ ions and their solvation shells. Its predicted IR activity renders it visible to FTIR measurements, and its frequency lies in the experimentally accessible range from 50 to 280 cm⁻¹. Our simulation yields a primary resonance frequency of 240 cm⁻¹ for this mode in simulations containing solvated Mg²⁺ ions (see Figure 4A). The experiment observes a corresponding IR active resonance in magnesium halide solutions at roughly 180 cm⁻¹ (see Figures 2 and 3). The shift of 60 cm⁻¹ is within the expected accuracy of a force field-based simulation. However, our assignment is further supported by similar resonance patterns, which are observed in the VDOS computed from the Cartesian velocities of Ca²⁺ and Sr²⁺ from the corresponding simulations. In addition to the ubiquitous 60 cm⁻¹ peak, we observe resonances at 170 and 100 cm⁻¹, respectively, for these ions as shown in Figure 5. In the case of Sr²⁺ this resonance appears as a shoulder of the 60 cm⁻¹ peak due to the similar frequency.

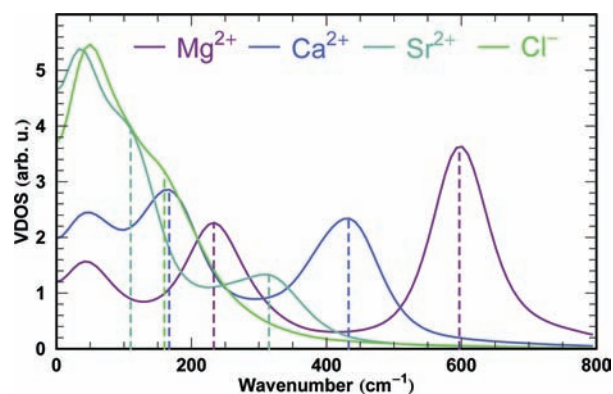


Figure 5. Simulated vibrational density of states (VDOS) computed from Fourier transformed velocity autocorrelation functions of divalent cations and chloride anions.

The resonances observed for these ions in the FTIR experiment in Figures 2 and 3 are found at 135–145 cm⁻¹ (CaCl₂ and CaBr₂) and 95–100 cm⁻¹ (SrCl₂ and SrBr₂). Hence, both the experimentally and simulated resonances follow a similar dependence on the ion mass (decreased resonance frequencies with increased ion mass). The simple dependence of the resonance frequency on the mass of the solvated ion supports the assignment of the underlying motion

to vibrational modes, which are similar to the Θ mode of the solvated Mg^{2+} .

A more detailed analysis of the vibrations of the heavier ions and their solvating water molecules in terms of symmetry-adapted normal modes is complicated by the decreased stability of the first solvation shells of these ions and the reduced symmetry. For example residence times of water molecules in the first solvation shell of Ca^{2+} are less than 100 ps.²⁵ A specific solvation shell of each is therefore only intact within short fragments of our simulated trajectories. In addition the coordination number is increased to an average of 6.7 water molecules in the first solvation shell. Despite these difficulties, we were able to adapt the vibrational analysis, which we carried out for Mg^{2+} ions and their solvation shells, to solvated Ca^{2+} ions (see SI).

In doing so, we can identify the 170 cm^{-1} resonance in the VDOS computed from Cartesian velocities of Ca^{2+} ions in Figure 5 to an IR active vibrational motion involving motion of the solvated ion against a part of its solvation shell, in agreement with the Θ mode observed for the Mg^{2+} ion. In correspondence to the analysis carried out for the solvated Mg^{2+} ion, we also find two Raman active resonances, which involve mostly Ca–O stretch motions, and a higher-frequency IR active mode.

In Figure 5 also the VDOS computed from Cartesian velocities of chloride counterions in the simulated salt solutions of divalent cations is shown. Also here, we find a pronounced resonance for the 60 cm^{-1} resonance assigned to the collective motions in water. In addition, we find a broad shoulder at $160\text{--}170\text{ cm}^{-1}$. While a direct comparison to the solvated cations cannot be made due to the different characteristics of the anion–water and cation–water interactions, the experimental observation of IR active resonances for all chloride salts at $190\text{--}200\text{ cm}^{-1}$, leads us also in this case to the assignment of this mode to a vibrational mode that involves motion of the solvated Cl^- anion against the H_2O molecules in its first solvation shell.

We note that, in addition to the experimentally observed IR modes of the cations with their hydration shells at frequencies below 280 cm^{-1} , our simulations also predict the existence of higher-frequency IR active modes, which follow a similar mass dependence. On the basis of the results of MD simulations we predict resonance frequencies of 600 , 440 , and 310 cm^{-1} for the modes of Mg^{2+} , Ca^{2+} , and Sr^{2+} ions with their solvation shells, respectively (Figures 4 and 5). The analysis in terms of symmetry-adapted normal modes also yielded Raman active modes at 200 and between 400 and 500 cm^{-1} for the Mg^{2+} ion and at 350 to 400 cm^{-1} for the Ca^{2+} . For Mg^{2+} , only the 480 cm^{-1} is predicted to have a strong Raman activity.²⁶ It should be pointed out that this Raman active mode has been observed previously at 350 cm^{-1} and assigned to Mg–O stretching motions, in agreement with our analysis.²² The red-shift of the experimentally observed Raman frequency with respect to the simulations presented here is very pronounced, but still within the expected accuracy for a force field based simulation: If we use the ratio between the experimentally observed and predicted Mg^{2+} band as scaling factor ($180\text{ cm}^{-1}/230\text{ cm}^{-1}$) we expect this band at 375 cm^{-1} which is very close to the experimentally observed Raman band.

While for Sr^{2+} the vibrational analysis in terms of symmetry-adapted normal modes has not been accomplished here, the existence of Raman-active Sr–O stretching vibrations between 250 and 350 cm^{-1} is likely, given the overall correspondence of

the observed vibrational features found for the simulated cations. In a symmetry-adapted picture, these motions involve primarily motion of the water molecules in the first solvation shell, leading to the absence of these features in the VDOS computed from Sr^{2+} ion velocities in Figure 5.

SUMMARY AND DISCUSSION

In summary, we have shown that the low-frequency (THz) frequency spectrum of a series of salt solutions can be well approximated by a linear superposition of concentration weighted neat water and ion contributions. The concentration dependence of the increase in THz absorption is found to be strictly linear. Both anion and cation bands can be assigned independently. The observation of clear resonances shows that the lifetime for the coupling between the water molecules in the hydration shell and the ions exceeds that of several vibrational cycles. The spectra display specific anion and cation resonances with frequencies that scale with the inverse ion mass and intensities that increase with increasing charge density. On the basis of accompanying MD simulations, these resonances have been unambiguously assigned to concerted rattling motions of the anion and cation with its first hydration shell. Whereas we find a very strong coupling of the ions with their first hydration shells, we do not observe any indication of long-ranged effects, which would hint to structure breaking, or structure making, or cooperative effects on water for atomic mono- and divalent salts. Furthermore, our present study underlines the need to include anion and cation contributions for a rigorous analysis of the THz spectrum of solvated salts. The ions which have been investigated here are ideal, prototypical systems, since they lack additional complications, e.g., steric effects and intramolecular vibrations and/or rotational/librational motions. The present study underscores the limited range of ion effects on their hydration shells. Thus, it contributes to a molecular-scale solution of the puzzle presented more than 100 years ago by Hofmeister concerning specific ion effects on myriad biochemical and physicochemical phenomena.

ASSOCIATED CONTENT

Supporting Information

Experimental details and data evaluation procedure on the p-Ge laser setup and the Fourier transform measurements; coefficient of determination for the fitting of data sets; comparison of the ionic absorption between mono- and divalent salts; computational details; trajectory analysis including the definition of the vibrational coordinates of the Mg ion and its solvation shell. This material is available free of charge via the Internet at <http://pubs.acs.org>.

AUTHOR INFORMATION

Corresponding Author

Martina.Havenith@rub.de

ACKNOWLEDGMENTS

We acknowledge E. Bründermann for fruitful discussions and scientific support. M.H. acknowledges financial support from BMBF Grants 05KS7PC2, 05K10PCA, and the Ruhr-University Bochum/MIWF. The work of G.N. was supported by the Ruhr-University Research School funded by Germany's Excellence Initiative [DFG GSC 98/1]. K.M.C and D.J.T. gratefully acknowledge financial support from the National Science Foundation (Grant CHE-0431512).

■ REFERENCES

- (1) Dalmas, O. *Biophys. J.* **2007**, *93*, 3729–3730.
- (2) Koneshan, S.; Rasaanah, J. C.; Lynden-Bell, R. M.; Lee, S. H. *J. Phys. Chem. B* **1998**, *102*, 4193–4204.
- (3) Hofmeister, F. *Naunyn-Schmiedeberg's Archives of Pharmacology*; Springer-Verlag: Berlin, New York, 1888; Vol. 25, pp 1–30.
- (4) Kunz, W., N. B.; Henle, J. *Curr. Opin. Colloid Interface Sci.* **2004**, *9*, 19–37.
- (5) Knipping, E. M.; Lakin, M. J.; Foster, K. L.; Jungwirth, P.; Tobias, D. J.; Gerber, R. B.; Dabdub, D.; Finlayson-Pitts, B. J. *Science* **2000**, *288*, 301–306.
- (6) Jungwirth, P.; Tobias, D. J. *Chem. Rev.* **2006**, *106*, 1259–1281.
- (7) Collins, K. D.; Washabaugh, M. W. *Q. Rev. Biophys.* **1985**, *18*, 323–422.
- (8) Tobias, D. J.; Hemminger, J. C. *Science* **2008**, *319*, 1197–1198.
- (9) Omta, A. W.; Kropman, M. F.; Woutersen, S.; Bakker, H. J. *Science* **2003**, *301*, 347–349.
- (10) Cappa, C.; Smith, J.; Wilson, K.; Messer, B.; Gilles, M.; Cohen, R.; Saykally, R. *J. Phys. Chem. B* **2005**, *109*, 7046–7052.
- (11) Smith, J. D.; Saykally, R. J.; Geissler, P. L. *J. Am. Chem. Soc.* **2007**, *129*, 13847–13856.
- (12) Schmidt, D. A.; Birer, Ö.; Funkner, S.; Born, B. P.; Gnanasekaran, R.; Schwaab, G. W.; Leitner, D. M.; Havenith, M. *J. Am. Chem. Soc.* **2009**, *131*, 18512–18517.
- (13) O'Brien, J. T.; Prell, J. S.; Bush, M. F.; Williams, E. R. *J. Am. Chem. Soc.* **2010**, *132*, 8248–8249.
- (14) Heisler, I. A.; Meech, S. R. *Science* **2010**, *327*, 857–860.
- (15) Tielrooij, K. J.; Garcia-Araez, N.; Bonn, M.; Bakker, H. J. *Science* **2010**, *328*, 1006–1009.
- (16) Bründermann, E.; Chamberlin, D.; Haller, E. *Appl. Phys. Lett.* **2000**, *76*, 2991–2993.
- (17) Perera, P. N.; Browder, B.; Ben-Amotz, D. *J. Phys. Chem. B* **2009**, *113*, 1805–1809.
- (18) Heugen, U.; Schwaab, G.; Bründermann, E.; Heyden, M.; Yu, X.; Leitner, D. M.; Havenith, M. *Proc. Natl. Acad. Sci. U.S.A.* **2006**, *103*, 12301–12306.
- (19) Ebbinghaus, S.; Kim, S. J.; Heyden, M.; Yu, X.; Gruebele, M.; Leitner, D. M.; Havenith, M. *J. Am. Chem. Soc.* **2008**, *130*, 2374–2375.
- (20) Niehues, G.; Heyden, M.; Schmidt, D. A.; Havenith, M. *Faraday Discuss.* **2011**, *150*, 193–207.
- (21) Dodo, T.; Sugawa, M.; Nonaka, E.; Honda, H.; Ikawa, S. *J. Chem. Phys.* **1995**, *102*, 6208–6211.
- (22) Callahan, K. M.; Casillas-Ituarte, N. N.; Roeselova, M.; Allen, H. C.; Tobias, D. J. *J. Phys. Chem. A* **2010**, *114*, 5141–5148.
- (23) Nath, N. S. N. *P. Indian AS-Math. Sci.* **1934**, *1*, 250–259.
- (24) Heyden, M.; Sun, J.; Funkner, S.; Mathias, G.; Forbert, H.; Havenith, M.; Marx, D. *Proc. Natl. Acad. Sci. U.S.A.* **2010**, *107*, 12068–12073.
- (25) Bockris, J. O., Reddy, A. K. N., Eds. *Modern Electrochemistry*; Kluwer Academic/Plenum Publishers: New York, 1998.
- (26) Wagner, N. L.; Wuest, A.; Christov, I. P.; Popmintchev, T.; Zhou, X.; Murnane, M. M.; Kapteyn, H. C. *Proc. Natl. Acad. Sci. U.S.A.* **2006**, *103*, 13279–13285.